

Simulating Wax Crayons

Dave Rudolf David Mould Eric Neufeld
dave.rudolf@usask.ca mould@cs.usask.ca eric@cs.usask.ca

Department of Computer Science
University of Saskatchewan

Abstract

We present a physically-inspired model of wax crayons, which synthesizes drawings from collections of user-specified strokes. Paper is represented by a height-field texture, and a crayon is modelled with a 2D mask that evolves as it interacts with the paper. The amount of wax deposition is computed based on the crayon contact profile, contact force, and friction. Previously deposited wax is smeared by crayon action, based on wax softness and contact information. The distributed wax is rendered using a simplified Kubelka-Monk model, which approximates light transmittance and scattering effects.

1 Introduction

Recent years have seen a proliferation of nonphotorealistic rendering styles, such as oil painting, pen-and-ink illustration, and copperplate engraving, among others. One thread of research has involved simulating specific traditional media, such as watercolours or pencils. In this paper, we propose a drawing primitive designed to mimic wax crayons.

Wax crayons possess certain characteristics making them challenging to model. The crayon contact area is large enough that the paper is not flat over the region of contact. The softness of wax is such that a substantial quantity of wax adheres to the page, and that previously deposited wax is smeared by the action of later crayon strokes. However, wax is much more viscous than paints and inks, and so its interactions are different than these other media. Also, the crayon footprint can change shape over a short period of time, changing substantially even within a single stroke. Many different colours of wax crayon are commonly in use, and the interaction between multiple translucent materials offers a rendering challenge.

We present a method for simulating wax crayons based on a physically-inspired model of wax deposition and smearing. Drawings are based on a collection of user-specified strokes; the effect at each point along a crayon's stroke is treated by first computing the crayon's contact profile, then depositing wax from the crayon to the paper, updating the crayon shape, and smearing previously deposited wax. The final distribution of wax is rendered with a simplified Kubelka-Monk model, which accounts for light transmission and scattering through multiple layers of wax.

Wax crayons are archetypally associated with a certain highly simplified drawing style. Despite the occasionally onerous physical simulation we describe, we have endeavoured to retain a sense of fun in the project, and we hope that this carries through in the childish artistic style of the images we present.

2 Previous Work

Originally, nonphotorealistic rendering (NPR) branched from work in image processing and pattern recognition circles. The earliest work in NPR consisted of specialized dithering techniques [24, 25]. Edge detection algorithms have been employed to decompose existing images or 3D models into their view-space elements: lines, curves, polygons, and the like [20, 7]. The purpose of such work was to emphasize the important features of an object, and remove distracting details and imperfections. From these basic building blocks, another area of NPR research emerged: that which aims to simulate a particular artistic style or medium, as we do in this paper. Graphical primitives are interpreted as artistic strokes or patches made by the simulated artistic medium. Previous work simulated media such as pencil sketches [20, 7] and drawings [13, 15, 21], charcoal drawings [14], watercolour[5], and stained glass [16]. Also, some work tries to simulate particular artistic styles, such as those of Dr. Seuss and Geoffrey Hayes [11].

Existing nonphotorealistic rendering methods follow

distinct branches. One such branch makes use of the aforementioned image processing techniques to extract primitives from 2D images and related data, such as depth buffers and stencil masks [20, 22]. Alternatively, 3D geometry can be used directly [15, 7, 14, 11]. Lastly, interactive systems depend on user-defined input [10, 5]. Our work falls into this category, although we have designed our model to facilitate other sources of geometry.

Techniques to represent artistic media vary widely, depending on the media being represented. A physically-based representation of paper has been developed [21], but 2D height maps are widely used to represent the high-level texture of paper. Since a crayon’s contact surface is relatively large, we also height maps to represent paper. With this approach, numerous texture synthesis methods have been employed to create visually appealing height maps [5, 17, 23]. We also make use of these methods.

In modelling actual artistic implements such as brushes and pencils, it is common practice to use a static one-dimensional height mask to represent a cross-section of the implement perpendicular to the stroke path [20, 7]. This simple representation limits the types of interaction that can be modelled. Some work uses texture mapping to simulate artistic media in an abstract sense [13, 14]. These methods assume that paper is relatively uniform and predictable in structure. Other research makes use of 2D masks to represent an implement [5, 10]. These models typically assume that the mask, once initialized, is static throughout its lifetime. Sousa and Buchanan [19] modelled graphite pencils using a polygon to represent the pencil tip. In their system, each vertex of the polygon is modified throughout the length of each stroke. Their method was used to represent a pencil that could rotate and pivot, and also have nonuniform pressure distributions. Points within the polygon must be interpolated from the surrounding vertices, so there is a limit to the kinds of profiles that can be represented. Most similar to our model is the work of Baxter et al [2], which makes use of polygon meshes to represent mainstream styles of artistic brushes. These meshes deform as the brush comes into contact with paper, accounting for spring tension in the bristles.

Finally, some methods require an explicit rendering step to generate the final image. There has been a great deal of research into volumetric rendering [12] and light scattering [9]. Takagi et al [21] used such methods to render their model of coloured pencils. A volumetric approach is the most flexible, allowing arbitrary views of the modelled medium. However, such an approach is also very costly. A convenient compromise is the Kubelka-Monk colour model, which has been used as an approximation for translucent pigments [8].

A deficiency of current rendering techniques is that they model some amount of simple pigment deposition, apply

the results to an incrementally developed image, and then start the next phase of deposition with an empty model [10, 5, 20, 7]. This eliminates the possibility of interaction between deposition phases. Sousa and Buchanan [19] have successfully modelled smudging of graphite pencil, but consider only a single pigment colour. Baxter et al [2] also allowed for some level of smearing. Existing pigment will either be “wet” and interact with the brush, or the pigment will be “dry”, and will not be considered for interaction.

There have been previous attempts at generating crayon-like images. Adobe Systems has included a *conté* crayon filter with their distributions of PhotoshopTM for some time [1]. This filter is simply a textured dither, and does not capture the true nature of wax. Kalnins et al [10] have used brush masks in a stroke-based system to deposit wax onto a paper model, but they do not account for interaction between layers of wax. Thus far, Corel’s Painter 8 [4] package has the most rigorous model of crayons. This system does model wax interaction, similar to the work of Baxter et al [2]. Corel’s model has two noticeable deficiencies. First, the colour model used is a purely subtractive model. When different colours of wax are blended, they do not appear as real wax does. Second, the wax deposited by each stroke is immediately mixed with any previously deposited stroke, and the brush absorbs the resulting colour. This would never occur with real crayons because of the high viscosity of wax. In this paper, we strive to eliminate these inconsistencies.

3 Modelling Wax

We are concerned with how a crayon leaves its trail of wax as it passes across the surface of paper. Many physical processes affect the crayon. We forego a rigid physical model, and concentrate on the more prominent natural effects; our representation of wax is based on observation. To understand the medium, we studied wax crayons using microscopy at different levels of magnification. Since wax tends to clump, most of our observations were done at relatively low magnification levels: between $6\times$ and $75\times$ zoom.

In this section, we present the basic components of our wax model. In particular, we discuss our representations of wax crayons and paper, as well as our process for generating paper texture. We then introduce the algorithm that describes the interaction between a crayon and a paper texture. This algorithm first determines the crayon’s vertical position with respect to the underlying paper and a scalar force. The crayon’s location is then used to smear wax previously deposited onto the paper, and also to deposit new wax. We then render the model using the Kubelka-Monk method.

3.1 Representation of Media

We follow traditional methods of representing paper as a 2D height map [20, 5]. Like recent work in NPR [19, 2, 21], our system must retain a record of deposited material throughout the evolution of the image. Because wax is easily smeared and carved, we must keep a dynamic model of wax as it adheres to a static paper texture.

To do so, we maintain a column of wax layers at each cell of the paper texture. The columns are normal to the gross plane of the paper. Each layer has its own *height*, *colour*, *light transmittance*, and *scattering* properties, which are used in our rendering algorithm (see section 4). For efficiency, adjacent wax layers with the same properties are blended together. Also, sufficiently thin layers are blended with adjacent layers. Layer blending helps prevent the proliferation of extremely thin layers, mostly caused by wax smearing (see section 3.6).

The actual crayon is modelled in a similar fashion. The profile of the crayon is also modelled as a 2D height map, where height values represent the crayon’s distance from the gross plane of the paper. Each cell in the crayon’s mask contains wax with the same colour, transmittance, and scattering properties. The 2D mask is modified as the crayon is worn down by friction.

This dynamic mask allows us to model a variety of profiles that real crayons would have. Using this method, we can represent not only a crayon’s sharpened edges as they are progressively abraded into a blunt shape, but also minor ridges and hollows that are carved by the features of the paper texture. We can also tailor our crayon height mask to represent sharpened and blunt crayon tips, the sharpened back-end rim, or even the long side of the crayon itself. Although the height map representation does prevent us from modelling some possible wax configurations (mainly, vertical concavities caused by extreme abrasion and adhesion), it is sufficient for modelling interactions with more widely-used media, such as paper, which is relatively flat.

3.2 Generation of Paper Texture

When generating final images of crayon drawings, it is important to consider paper texture. Although our deposition and smearing methods do not require a particular texture, they do depend on the texture. Real paper textures vary widely. Ideally, we should choose a texture that approximates a kind of paper that is associated with wax crayons. In consequence, we have striven to find a height field texture which is quite rough, akin to an inexpensive construction paper.

We used the lunar texture postulated by van Wijk [23], which has a suitable combination of roughness and coherence. Our version of this texture was generated by convolv-

ing a quarter-circle arc with a lattice populated by uniform noise. An example of the texture thus derived is shown in Fig. 1.

Our deposition and smearing algorithms (see section 3.3) require that some texture be provided, but make no assumptions about the nature of that texture. To test this aspect of our model, we have also generated textures that are fundamentally different than the fore-mentioned lunar texture. We do so by using 2D masks to scale the amplitude of uniform noise. This mask is tiled across the noise lattice to impose a repetitive structure upon the generated texture. An example of one such texture is seen in Fig. 1.

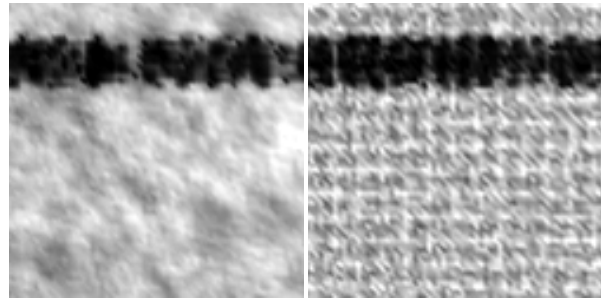


Figure 1. Wax deposition with lunar convolution and stipple restriction masks, respectively.

3.3 High-Level Interaction Algorithm

To model crayons, we observe how real crayons interact with the underlying paper. First, we note that wax is deposited by the crayon. The volume of deposited wax depends on the size of the contact area between the crayon and paper, the slope of the paper over that area, and the crayon force. Second, wax that has been deposited onto the paper can be smeared around when the crayon passes over it. This smearing process pushes wax from the peaks of the paper texture, and down into adjacent lower regions. Smearing also has a directional component, in that the crayon can push wax over ridges in the paper. Fig. 2 illustrates the interactions of a crayon with the paper texture.

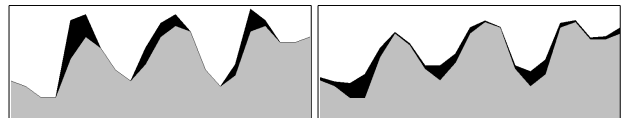


Figure 2. Hypothetical interaction between crayon and paper: (left) Wax deposition, (right) Smearing.

When creating wax renditions, we use lines as our only drawing primitive, although artists who work with acrylic crayons have other techniques at their disposal. To draw a line, we consider the endpoints P_1 and P_2 , the crayon's height mask M , the scalar force f applied by the crayon to the paper, and the set C of colour properties of the wax. For any given crayon position, we must prepare the crayon, and modify the wax model. First, we adjust the crayon height values with respect to the applied force, the crayon's height profile, and the profile of the paper at the current location. We then use the new height values to modify the set of wax layers L that lie on the paper. In modifying these layers, we first smear wax that is already deposited on the paper at the current location, then deposit new layers onto the paper. This process is summarized in Fig. 3.

```

proc drawLine(  $P_1, P_2, M, C, f, L$  )
  for each point  $P_i$  on the line segment  $P_1P_2$ 
    adjustCrayonHeight(  $P_i, M, f, L$  )
    smearExistingWax(  $P_i, P_1P_2, M, L$  )
    addNewWax(  $P_i, P_1P_2, f, M, C, L$  )
  end
end

```

Figure 3. Summary of the actions taken when a line is drawn.

Of course, to draw a line, we only choose points P_i that are appropriate for the resolution of our paper texture. In the following sections, we give detailed algorithms for each of the above procedures.

3.4 Crayon Compression Due To Force

When drawing a line with a crayon, we must remove some volume of wax from the crayon and deposit it onto the paper underneath. The volume of deposited wax depends on the values of the crayon's height mask, relative to the local height of the paper. The difference between these heights determines how much wax is deposited, as well as how much wax is smeared from that region of the paper onto adjacent regions.

Since the crayon's cells will potentially be worn away with each movement, we must adjust the crayon's overall height at each step so that, at the next step, the crayon is exerting the same amount of force upon the paper. To do so, we assume that the wax compresses linearly, and use Hooke's Law of Compression to numerically determine the appropriate vertical displacement.

Hooke's Law [6] can be written

$$F = Y \frac{\Delta L}{L_0} A, \quad (1)$$

where Y is Young's modulus, ΔL is the amount of compression, L_0 is the unstressed length, and A is the cross-sectional area. If we assume that the length of the crayon L_0 is approximately constant, being much greater than the change in length ΔL , then we can reduce the above equation to:

$$F = \lambda A \Delta L. \quad (2)$$

For the constant λ , we simply choose a value that produces aesthetically pleasing results.

We can sum up the force contributed by each crayon cell onto its corresponding paper cell, setting the contribution to 0 if the crayon cell is above its paper cell. This latter step prevents us from calculating the crayon's displacement directly, as we no longer have a linear function to evaluate. Instead, we use a binary search algorithm to find a displacement that gives us the desired amount of force, within some tolerance ϵ . To do so, we consider the height $h_{m_{ij}}$ of the crayon at each mask cell m_{ij} , and the height of the paper $h_{p_{ij}}$ at the corresponding location P_{ij} ; the crayon height calculation is summarized in Fig. 4. As seen in Fig. 5, the amount of deposited wax varies with the applied force.

```

proc adjustCrayonHeight(  $P, M, f, L$  )
   $h_{min}^{crayon} \leftarrow \min(\forall h_{m_{ij}} : m_{ij} \in M)$ 
   $h_{min} \leftarrow \min(\forall h_{p_{ij}} : m_{ij} \in M \text{ and } P_{ij} = P + (i, j))$ 
   $h_{max} \leftarrow \max(\forall h_{p_{ij}})$ 
  while  $h_{max} - h_{min} > \Delta$ 
     $h_{mid} \leftarrow (h_{max} + h_{min}) / 2$ 
     $f_{h_{mid}} \leftarrow 0$ 
    for each  $m_{ij} \in M$ 
       $\delta h = h_{p_{ij}} + h_{L_{P_{ij}}} - (m_{ij} - h_{min}^{crayon} + h_{mid})$ 
      if  $\delta h > 0$ 
         $f_{h_{mid}} \leftarrow f_{h_{mid}} + \lambda \delta$ 
      end
    end
    if  $f < f_{h_{mid}}$ 
       $h_{min} \leftarrow h_{mid}$ 
    else
       $h_{max} \leftarrow h_{mid}$ 
    end
   $h_{mid} \leftarrow (h_{max} + h_{min}) / 2$ 
  for each  $M_{ij}$ 
     $M_{ij} \leftarrow M_{ij} - h_{min}^{crayon} + h_{mid}$ 
  end
end

```

Figure 4. Calculation of the crayon height values.

Having positioned the crayon, we can then process its interaction with the paper.

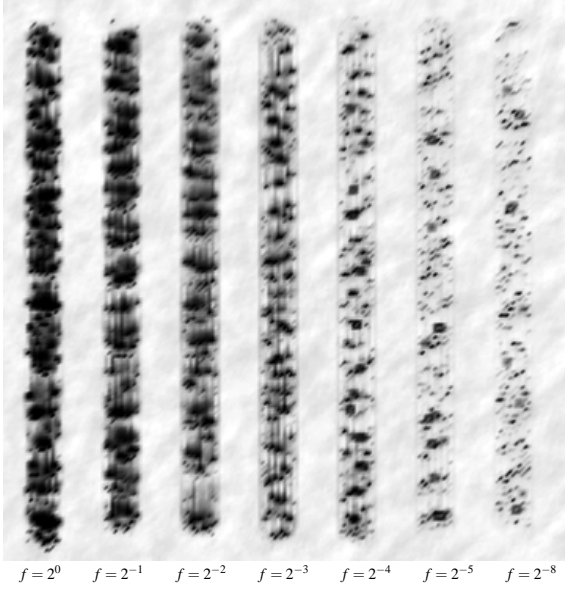


Figure 5. Wax deposition with different amounts of force.

3.5 Frictional Deposition

Friction is the process by which wax is broken from the crayon and deposited onto the paper. We model friction on two levels, macroscopic and microscopic. On a macroscopic level, we are concerned with the force of the crayon normal to the surface of the paper. As the crayon encounters convex features in the paper's texture, it leaves behind some quantity of wax. On a microscopic level, we use a coefficient of friction to approximate the roughness of the paper on a smaller scale. The amount of wax should be proportional to the frictional force.

$$\vec{F}_F = \mu \vec{F}_N = \mu \vec{N} \frac{\vec{N} \cdot \vec{F}_C}{\|\vec{N}\| \|\vec{F}_C\|} \quad (3)$$

where

\vec{F}_C is the force of the crayon on the feature's surface,

\vec{F}_F is the force of friction,

\vec{F}_N is the crayon force normal to the feature's surface,

\vec{N} is the surface normal of the feature, and

μ is the coefficient of friction for the paper.

With our height-mapped paper texture, we interpolate adjacent height values to define a plane against which the crayon is moving, and calculate friction with respect to that plane.

The value of μ depends on whether the crayon is interacting with clean paper or with paper that already has some

wax. To add to the complications, a region of paper with an extremely thin layer of wax will have different frictional properties than a region with a thicker layer of wax. Current literature on the production of pulp and paper has little to suggest an appropriate coefficient for paper alone. While tribology does offer insight into the wear properties of polymers and resins [3, 18], it is difficult to determine the ratios of esters, fatty acids, alcohols and hydrocarbons present in wax crayons. Since our model is not rigorously analytical, we artistically choose the two friction coefficients, and smooth the transition between them for thin layers of wax.

To deposit wax, we consider the point P at which the crayon is located, the crayon's directional heading \vec{V} , the crayon's height mask M and its height values m_{ij} , the set of colour properties C of the crayon, and scalar force f which is normal to the gross plane of the paper. The wax deposited at each point P_{ij} is added to the set of layers $L_{P_{ij}}$ at that point. An example of wax deposition using our model is shown in Fig. 8. The method for computing deposition appears in Fig. 6.

```

proc addNewWax(  $P, \vec{V}, M, C, f, L$  )
   $\bar{V} \leftarrow \vec{V} / \max(x_{\vec{V}}, y_{\vec{V}})$ 
  for each  $m_{ij} \in M$ 
     $P_{ij} \leftarrow P + (i, j)$ 
     $P'_{ij} \leftarrow P_{ij} + \bar{V}$ 
     $\vec{S}_{ij} \leftarrow (x_{\vec{V}}, y_{\vec{V}}, h_{P'_{ij}} - h_{P_{ij}})$ 
     $\vec{F}_{ij} \leftarrow (x_{\vec{V}}, y_{\vec{V}}, -f)$ 
     $\alpha \leftarrow 1 / (1 + h_{P'_{ij}}^{wax})$ 
     $\mu_{ij} \leftarrow \alpha \mu_{paper} + (1 - \alpha) \mu_{wax}$ 
     $\delta h_{P'_{ij}}^{wax} \leftarrow \mu (h_{P'_{ij}} - m_{ij}) \sin(\vec{S}_{ij}, \vec{F}_{ij})$ 
     $m_{ij} \leftarrow m_{ij} + \delta h_{P'_{ij}}^{wax}$ 
     $L_{P_{ij}} = L_{P_{ij}} + \{(\delta h_{P'_{ij}}^{wax}, C)\}$ 
  end
end

```

Figure 6. The method for moving wax from the crayon to the paper.

3.6 Smearing

Smearing is a characteristic of wax in the same way as bleeding is a characteristic of watercolours. As a crayon moves across paper, it smears the wax into adjacent regions. Both newly and previously deposited wax are smeared. region, it will force wax from that region to spread to adjacent regions. To simulate smearing, we employ a smearing mask that encompasses the current paper cell and its eight neighbors. Each value in the mask determines the proportion of

wax that is to be moved from the current cell to the cell underneath the given mask location.

To generate this mask, we consider the relative location of each value, the height of the paper (and its wax) at that location, and the directional heading of the crayon. Mask elements are given by the following equation:

$$S_{xy} = \frac{1}{\|(x,y)\|} \left(\alpha \Delta z + \beta \cos((x,y), \vec{V}_C) \right). \quad (4)$$

We set the center mask value $S_{0,0}$ to zero, so that we avoid “smearing” wax back onto itself.

The values of α and β can be chosen to match a particular smear pattern, or can be proportional to the crayon’s scalar velocity. Once the mask is constructed, it is normalized to a wax viscosity factor v . The wax is then removed from the current paper cell, and distributed to its neighbors according to their mask values. Smearing is summarized in Fig. 7. Some results from our smearing algorithm are shown in Fig. 8.

```

proc smearExistingWax(  $P, \vec{V}, M, L$  )
  for each  $m_{ij} \in M$ 
     $S$  is a  $3 \times 3$  matrix.
    for each  $s_{mn} \in S$ 
       $s_d \leftarrow \cos(\vec{V}, (m, n))$ 
       $s_f \leftarrow (h_{P_{ij}} + h_{L_{P_{ij}}}) - (h_{P_{(i+m)(j+n)}} + h_{L_{P_{(i+m)(j+n)}}})$ 
       $s_{mn} \leftarrow \max\{0, s_{directional} + s_{height}\}$ 
    end
     $S \leftarrow vS / (\sum s_{mn})$ 
     $\delta h_{wax} \leftarrow h_{L_{ij}}(h_{L_{P_{ij}}} + h_{P_{ij}} - m_{ij})$ 
     $L_{P_{ij}'} \leftarrow \{l_a, \dots, l_n\} : \sum h_{l_i} = \delta h_{wax}$ 
    for each  $s_{mn} \in S$ 
      for each  $l_i \in \delta L_{P_{ij}'}$ 
         $L_{(i+m)(j+n)} \leftarrow L_{(i+m)(j+n)} + s_{mn} l_i$ 
      end
    end
  end
end

```

Figure 7. Pseudocode for the smearing algorithm.

3.7 Parameters of the Model

Although we have not attempted to construct a thorough physical simulation of wax, our model is quite flexible. There are various parameters in the system, of which we can make use to represent other artistic media. Table 1 summarizes these parameters and gives the values we used.

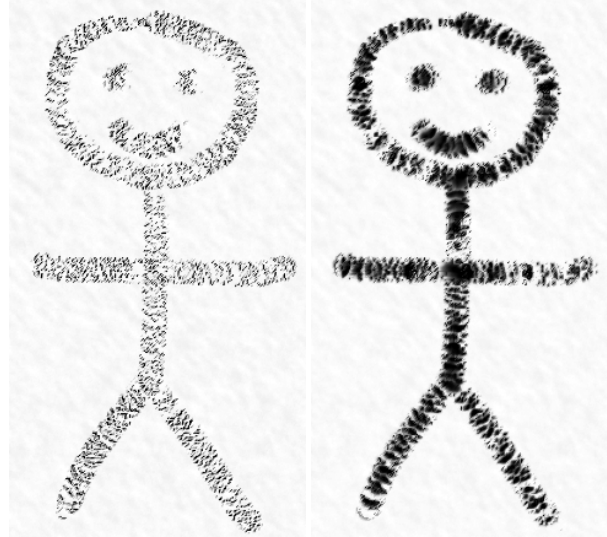


Figure 8. Modelled interaction between crayon and paper: (left) Wax deposition, (right) Smearing.

| Symbol | Description | Value |
|---------------|------------------------------------|--------------|
| μ_{wax} | Frictional coefficient of wax. | 0.5 |
| μ_{Paper} | Frictional coefficient of paper. | 2 |
| v | Viscosity of wax. | 0.5 |
| α | Flow smear factor. | 0.2 |
| β | Directional smear factor. | $1 - \alpha$ |
| λ | Wax compression resistance factor. | 0.0005 |
| ϵ | Force accuracy factor. | $\lambda/4$ |

Table 1. Parameters of our model.

4 Rendering

We next turn our attention to generating images from the wax model. Wax is best treated as a translucent pigment, so simple additive and subtractive colour models such as RGB and CMY are inadequate. Instead, we employ a simplified Kubelka-Monk (KM) model [8]. The KM model approximates spectral *transmittance*, *scattering*, and *interference*. The value of these properties can be inferred by two specified colours [5]. Each of these colours is the observed result of a layer of pigment overtop of uniform background: one is the result with a black background, and the other with a white background. From these two results, KM theory provides a means of interpolating the resulting colour, given arbitrary backgrounds. The KM model does so by inferring how much light is scattered by the pigment medium, and how much is transmitted through the medium. The KM model also approximates changes in hue due to thin-film

interference.

In our model, we ignore interference effects, as we did not observe them to contribute significantly to real crayon drawings. Consequently, each crayon is associated with a single RGB *colour* property, as well as *transmittance* and *scattering* factors. These factors apply equally to all three colour channels.

As mentioned previously, extremely thin layers are merged together. The optical properties of the resulting layer are set to weighted averages of the two layers that were merged. The weight for each layer is proportional to that layer’s height. This is a gross simplification of the KM model, but still produces acceptable results and significantly increases performance of the smearing algorithm.

To render the wax model, we consider the colour of the paper texture $C_{T_{ij}}$ at each point P_{ij} on the paper. To calculate the colour that results from a layer of wax l_k , we make use of the layer’s colour C_{l_k} , its transmittance t_{l_k} , and its reflectance r_{l_k} . Details of the calculation are given in Fig. 9.

```

proc render(  $T$  )
  for each point  $P_{ij}$  on the paper texture  $T$ 
    Colour  $C_{ij} \leftarrow C_{T_{ij}}$ 
    for each wax layer  $l_k$  at point  $P_{ij}$ 
       $C_{ij}^{transmit} \leftarrow (t_{l_k} C_{l_k})^{h_{l_k}} C_{ij}$ 
       $C_{ij}^{scatter} \leftarrow 1 - (1 - C_{l_k})^{r_{l_k} h_{l_k}}$ 
       $C_{ij} \leftarrow C_{ij}^{transmit} + C_{ij}^{scatter}$ 
    end
  end
end

```

Figure 9. Our simplified Kubelka-Monk rendering algorithm.

We have endeavored to duplicate the optical properties of common children’s crayons. Fig. 10 illustrates the optical properties of our generated crayons, as compared to real wax crayons. Table 2 lists the crayons we simulated and their empirically determined properties.

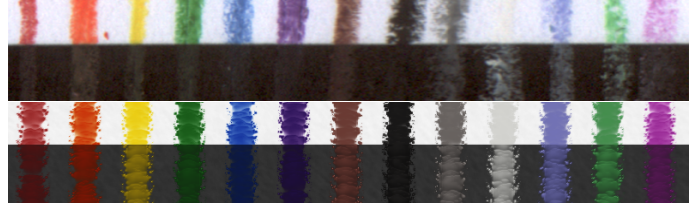


Figure 10. Appearance of (top) real wax crayons, and (bottom) our generated crayons.

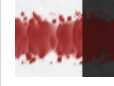
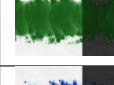
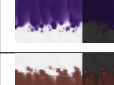
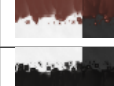
| Crayon | Colour | R | G | B | T | S |
|---|------------|-------|------|-------|--------|-------|
|  | red | 0.95 | 0.45 | 0.45 | 0.605 | 0.051 |
|  | orange | 0.999 | 0.55 | 0.2 | 0.605 | 0.042 |
|  | yellow | 0.95 | 0.9 | 0.2 | 0.715 | 0.111 |
|  | green | 0.35 | 0.8 | 0.35 | 0.385 | 0.096 |
|  | blue | 0.3 | 0.5 | 0.9 | 0.715 | 0.054 |
|  | purple | 0.65 | 0.4 | 0.9 | 0.385 | 0.06 |
|  | brown | 0.8 | 0.55 | 0.5 | 0.3025 | 0.15 |
|  | black | 0.26 | 0.25 | 0.245 | 0.11 | 0.24 |
|  | grey | 0.42 | 0.4 | 0.39 | 0.44 | 0.51 |
|  | white | 0.8 | 0.8 | 0.79 | 0.55 | 0.33 |
|  | periwinkle | 0.7 | 0.7 | 0.9 | 0.385 | 0.21 |
|  | sea green | 0.6 | 0.9 | 0.65 | 0.33 | 0.15 |
|  | orchid | 0.85 | 0.4 | 0.84 | 0.66 | 0.09 |

Table 2. Optical properties of simulated crayons.



Figure 11. Sample images (right) generated from user defined strokes (left).

5 Results

Fig. 11 shows examples of final images. In the first image, interaction between colours is visible, particularly at the edges of the man’s tie. We can also see the effects of differing friction on the man’s shirt: the periwinkle crayon was applied first, and when the sea-green crayon was used it preferentially deposited wax in regions which had been bare. Interaction between colours is also apparent in the second image, particularly in the red and yellow portions of the character’s hair, and on the polkadots of the pajamas. This image also demonstrates the scattering component of our KM model: the crayons’ colours are visible even when the background is black.

Although efficiency was not our primary concern, we did not want to impose long rendering times on the user. Our model is not efficient enough for use in a real-time rendering pipeline. It is suitable for interactive stroke-based applications, provided that the user has a high-end workstation. Depending on line length, crayon contact area, and amount of force, rendering each crayon stroke requires between 0.3 and two seconds on a 2.4GHz Pentium 4.

For conventional home PCs, our model could be used for an effective preview-and-render system. Since the smearing method is the most costly part of our algorithm, we can dramatically increase speed by removing this effect for previews, at the cost of dramatically changing the resulting image. Perhaps a better compromise between speed and realism is to simply decrease the resolution of the preview image, and also scale the crayon mask’s size and the stroke coordinates accordingly. This will still include smearing effects, and give a good estimate of the final image.

6 Conclusions and future work

We presented a physically inspired model of wax crayons that extends previous work by representing crayons as dynamic 2D height masks. This approach allows us to more accurately model crayon wear as it interacts with paper.

Images are generated with user-defined strokes as primitives. Each stroke deposits wax on the paper, and at each point we also model the crayon’s interaction with previously deposited wax. The final distribution of wax is rendered using Kubelka-Monk, treating the wax as a collection of plane parallel layers.

We show some images generated by the model, revealing both strengths and weaknesses. Overall, the images resemble crayon drawings. The erratic placement of wax within the bounds of a stroke is captured. However, there are phenomena not captured by the model. Real crayons are affected by small particles of dirt or dust, or even small hard pieces of wax embedded in the softer surrounding material,

which causes specks and tracks in the strokes. We made no attempt to include this effect in our model.

Although our model is not presently fast enough for real-time rendering, it can be used for interactive drawing applications with powerful hardware. We are presently investigating simplifications and optimization.

Our model produces acceptable results for crayons with near-solid viscosity (e.g., children’s wax crayons). However, softer media, such as acrylics and pastels, would require a more complex smearing mechanism. Our smearing mechanism only considers the effects of a single grid cell and its eight neighbors, while with real pastels, pressure would be propagated a greater distance. Although the same thing can be said about wax, it is a much more viscous substance, and so we assume that the vast majority of the pressure is absorbed by the immediate neighbors. Such an assumption would not hold for pastels.

We do not account for some phenomena present in real crayon drawings. First, and most prevalent, real wax does not wear as discretely as we have modelled it. Wax is a self-adhesive substance, and so when it is removed from one region of a crayon’s tip, it may bring along wax from adjacent regions. Similarly, when a crayon moves across a thick layer of wax residing on the paper, it tends to carve away large clumps of wax. To add to complications, these clumps can be pressed to the tip of the crayon, and may be carried great distances before being released back to the paper. At present, our model has no means of simulating this.

Refinements to our model would make it more generally applicable, both to modeling wax crayons and to related media such as acrylics. We have only marginally accounted for the orientation of the crayon itself. We could incorporate more complicated mechanics by using methods such as those of Sousa [19].

Much work still remains in simulating the predominant drawing style associated with wax crayons. Some existing work tries to model the imperfect stroke patterns that humans produce [20, 7, 15], but we are aware of no work on modelling the drawing styles of children.

Future work also lies in connecting our stroke primitive with a system automatically deploying strokes. The combined system would provide a wax crayon filter, turning out crayon renditions of arbitrary 2D images, or from 3D geometry.

Acknowledgements

Special thanks to Nicole Haddock, Denyse Klette, and the rest of the Belly Button BuddiesTM for allowing us to scribble on their illustration.

References

- [1] Adobe Systems Incorporated, New York, NY, USA. *Adobe Photoshop 6 User's Manual*, 2001.
- [2] B. Baxter, V. Scheib, M. C. Lin, and D. Manocha. Dab: interactive haptic painting with 3d virtual brushes. In *Proceedings of the 28th annual conference on Computer graphics and interactive techniques*, pages 461–468. ACM Press, 2001.
- [3] B. Bhushan and B. K. Gupta. *Handbook of tribology: materials, coatings, and surface treatments*. McGraw-Hill, New York, NY, USA, 1991.
- [4] Corel Corporation, Ottawa, ON, Canada. *Corel Painter 8 User's Guide*, 2003.
- [5] C. J. Curtis, S. E. Anderson, J. E. Seims, K. W. Fleischer, and D. H. Salesin. Computer-generated watercolor. In *Proceedings of the 24th annual conference on Computer graphics and interactive techniques*, pages 421–430. ACM Press/Addison-Wesley Publishing Co., 1997.
- [6] J. D. Cutnell and K. W. Johnson. *Physics*. John Wiley and Sons, Inc., New York, NY, USA, 3rd edition, 1995.
- [7] B. Gooch and A. Gooch. *Non-photorealistic rendering*. A.K. Peters, Ltd, New York, NY, USA, 2001.
- [8] C. S. Haase and G. W. Meyer. Modeling pigmented materials for realistic image synthesis. *ACM Transactions on Graphics (TOG)*, 11(4):305–335, 1992.
- [9] H. W. Jensen, S. R. Marschner, M. Levoy, and P. Hanrahan. A practical model for subsurface light transport. In *Proceedings of the 28th annual conference on Computer graphics and interactive techniques*, pages 511–518. ACM Press, 2001.
- [10] R. D. Kalnins, L. Markosian, B. J. Meier, M. A. Kowalski, J. C. Lee, P. L. Davidson, M. Webb, J. F. Hughes, and A. Finkelstein. WYSIWYG NPR: drawing strokes directly on 3d models. In *Proceedings of the 29th annual conference on Computer graphics and interactive techniques*, pages 755–762. ACM Press, 2002.
- [11] M. A. Kowalski, L. Markosian, J. D. Northrup, L. Bourdev, R. Barzel, L. S. Holden, and J. F. Hughes. Art-based rendering of fur, grass, and trees. In *Proceedings of the 26th annual conference on Computer graphics and interactive techniques*, pages 433–438. ACM Press/Addison-Wesley Publishing Co., 1999.
- [12] P. Lacroute and M. Levoy. Fast volume rendering using a shear-warp factorization of the viewing transformation. In *Proceedings of the 21st annual conference on Computer graphics and interactive techniques*, pages 451–458. ACM Press, 1994.
- [13] A. Lake, C. Marshall, M. Harris, and M. Blackstein. Stylized rendering techniques for scalable real-time 3d animation. In *Proceedings of the first international symposium on Non-photorealistic animation and rendering*, pages 13–20. ACM Press, 2000.
- [14] A. Majumder and M. Gopi. Hardware accelerated real time charcoal rendering. In *Proceedings of the second international symposium on Non-photorealistic animation and rendering*, pages 59–66. ACM Press, 2002.
- [15] A. Mohr and M. Gleicher. Hijackgl: reconstructing from streams for stylized rendering. In *Proceedings of the second international symposium on Non-photorealistic animation and rendering*, pages 13–ff. ACM Press, 2002.
- [16] D. Mould. A stained glass image filter. *Proceedings of the Eurographics Symposium on Rendering 2003*, 16(1):20–25, June 2003.
- [17] K. Perlin. An image synthesizer. In *Proceedings of the 12th annual conference on Computer graphics and interactive techniques*, pages 287–296. ACM Press, 1985.
- [18] Plastics Design Library, Norwich, NY, USA. *Fatigue and tribological properties of plastics and elastomers*, 1995.
- [19] M. C. Sousa and J. W. Buchanan. Computer-generated graphite pencil rendering of 3D polygonal models. *Computer Graphics Forum*, 18(3), 1999.
- [20] T. Strothotte and S. Schlechtweg. *Non-photorealistic computer graphics: modelling, rendering, and animation*. Morgan Kaufmann, Natick, MA, USA, 2002.
- [21] S. Takagi, M. Nakajima, and I. Fujishiro. Volumetric modelling of colored pencil drawings. *Pacific Graphics*, October 1999.
- [22] S. M. F. Treavett and M. Chen. Pen-and-ink rendering in volume visualisation. In *Proceedings of the conference on Visualization '00*, pages 203–210. IEEE Computer Society Press, 2000.
- [23] J. J. van Wijk. Spot noise: Texture synthesis for data visualization. *Computer Graphics (Proceedings of SIGGRAPH 91)*, 25(4):309–318, July 1991. ISBN 0-201-56291-X. Held in Las Vegas, Nevada.
- [24] L. Velho and J. de Miranda Gomes. Digital halftoning with space filling curves. In *Proceedings of the 18th annual conference on Computer graphics and interactive techniques*, pages 81–90. ACM Press, 1991.
- [25] O. Vevyovka and J. Buchanan. Halftoning with image-based dither screens. *Graphics Interface*, pages 167–174, June 1999.